Solar water oxidation by multi-component TaON photoanodes functionalized with nickel oxide

Satnam Singh Gujral,[a] Alexandr N. Simonov,*[a] Xi-Ya Fang,[b] Masanobu Higashi,[c] Ryu Abe[c] and Leone Spiccia*[a]

Abstract: Efficient solar-powered water oxidation over the TaON-based anodes requires coupling this photoactive *n*-type semiconductor to an electrooxidation catalyst to improve the otherwise unsatisfactory activity and stability. Herein, we examine how functionalization with electrodeposited nickel oxide, NiO_x, affects the performance of screen-printed TaON photoanodes post-necked with titania (TiO_2-TaON). The effects of the NiO_x photo-electrodeposition parameters on the microstructure and photo-catalytic performance of the resulting anodes are explored. Enhancements in the transient water oxidation photocurrent densities by 6-fold *vs*. unmodified TiO_2-TaON were achieved with the use of the NiO_x/TiO_2-TaON photoanodes. Long-term stability tests reveal a slow but persistent degradation of the performance of the multicomponent photocatalysts under the severely oxidizing conditions of water photo-oxidation coincident with continuous morphological changes in the NiO_x deposits.

Introduction

Solar-powered water splitting is currently gaining a momentum as a viable technology for capturing intermittent solar energy in a storable and transportable form, *viz.* in the chemical bonds of molecular hydrogen.[1] The photo-electrochemical concept of water decomposition, where a semiconductor photocatalyst generates electron-hole pairs to drive hydrogen and oxygen evolution half-reactions at spatially separated electrodes is attracting growing attention due to a range of potential advantages.[2] Arguably, the most attractive feature of the photo-electrochemical approach is a comparatively simple single-unit design of a bi-functional electrode assembly, which both absorbs light and catalyzes the half-reactions and does not need to be integrated into a more complex modular system. However, these specifics also place a number of strict constraints on the semiconductor catalyst material, and truly efficient catalysts for photo-electrochemical water splitting are yet to be discovered.[3]

It comes as no surprise that the band structure is the principal property of a semiconductor that must meet several strict requirements in order for the photocatalyst to be capable of sustaining water splitting powered by sunlight (Scheme 1). Firstly, a narrow band gap (E_G < 3 eV) is needed for absorption of visible and near-IR photons (λ > 400 nm), which make a major contribution to sunlight incident on the surface of our planet.[3a, 4] Secondly, E_G must be wider than 1.6 eV to provide sufficient photopotential needed to overcome sluggish kinetics of water splitting, mainly of the oxygen evolution half-reaction.[5] Thirdly, the conduction and valence band levels must be positioned at higher and lower energies than those corresponding to the hydrogen evolution reaction (HER) and the oxygen evolution reaction (OER), respectively.[2d, 3c, 6] If a highly robust, abundant and non-toxic semiconductor complying with the above conditions can be developed, which at the same time catalyzes either the OER (*n*-type) or the HER (*p*-type), then the search for an ideal photo-electrocatalyst can be considered accomplished. To date, none of the materials or combinations of materials discovered strictly meet all of these requirements.

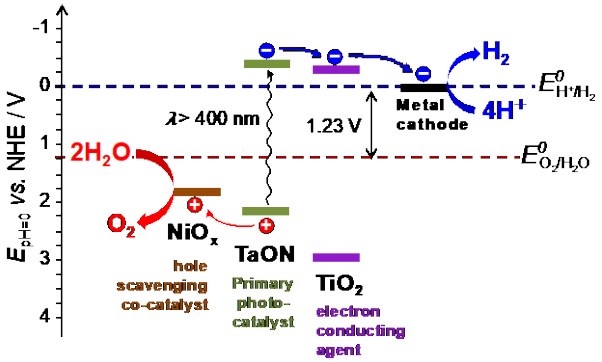

Scheme 1. Schematic of the charge transfer processes occurring during solar-driven water splitting at the TaON photoanode modified with TiO_2 (electron conducting agent) and NiO_x (hole scavenging co-catalyst).

Among the many inorganic photocatalysts applied for water splitting (TiO_2,[7] WO_3,[8] ZnO,[9] α-Fe_2O_3[10], $BiVO_4$,[11] *etc.*), tantalum-based oxynitrides[3b, 12] are one of few *n*-type semiconductors with close to an ideal electronic configuration, as illustrated in Scheme 1. However, TaON has an intrinsically poor catalytic activity for the OER, and even more importantly, unsatisfactory stability as a photocatalyst. As suggested in previous reports,[3b, 12e, 13] TaON and other oxynitrides undergo oxidative self-degradation under irradiation, which deteriorates the water photo-oxidation performance rapidly. This degradation process can be attributed to interactions of the photo-generated holes with N^{3-} to produce molecular N_2 and visible light insensitive Ta_2O_5 (E_G = 3.9 eV). There are also high recombination losses in TaON, which limit the onset potential for the appreciable photo-electrocatalyzed OER to >1.2 V *vs.* reversible hydrogen electrode (RHE; hereinafter all potentials are reported *vs*. this reference).[12e, 14]

Partial remediation of inefficient charge-separation in tantalum oxynitride is possible *via* modification of the photoanodes with electron-conducting coatings (TiO_2,[14-15]

[a] *Mr. S. S. Gujral, Dr. A. N. Simonov,* Prof. Dr. L. Spiccia**
School of Chemistry and the ARC Centre of Excellence for Electromaterials Science
Monash University, Victoria, 3800, Australia.
E-mail: alexandr.simonov@monash.edu; leone.spiccia@monash.edu
[b] *Dr. X. Y. Fang*
Monash Centre for Electron Microscopy,
Monash University, Victoria, 3800, Australia.
[c] *Dr. M. Higashi, Prof. Dr. R. Abe*
Department of Energy and Hydrocarbon Chemistry, Graduate School of Engineering
Kyoto University, Kyoto 615-8510, Japan.

Supporting information for this article is given via a link at the end of the document.

Ta_2O_5[13a] or TaON[12e, 13a]) similarly to the post-necking applied in the dye-sensitized solar cell technology,[16] and through the use of hole-scavenging water oxidation electrocatalysts (IrO_2,[12e, 13a] CoO_x,[13c, 17] RhO_x,[12f] MnO_x[18] and $CaFe_2O_4$[19]). Apart from improvements in charge separation, the electrocatalysts significantly enhance the rates of the OER. When applied together (Scheme 1), post-necking and water oxidation co-catalysts improve the water photo-oxidation activity of the TaON-based anodes by up to three orders of magnitude. Expectedly, the synthetic methods used affect the microstructure and location of the promoting charge-transfer agents on the TaON surface, which are of paramount importance for the resulting performance of the photoanode.[20], [21] To achieve efficient charge-separation, the electron-conducting coatings and hole-scavenging electrocatalysts should ideally cover the photoactive TaON surface homogeneously. However, excessive loadings of the modifiers are detrimental, mainly due to suppression of the light absorption by tantalum oxynitride, so that thin necking layers and highly dispersed co-catalyst particles are highly desirable.[12e, 13c, 17] Recently, we demonstrated the simple and efficient functionalization of the TiO_2-coated TaON photoanodes (hereinafter, TiO_2-TaON) with MnO_x[18] or CoO_x[17] nanoparticles by using photo-assisted electrodeposition. Irradiation of TiO_2-TaON in contact with M^{2+} solutions facilitates formation of the highly-dispersed MO_x particles on the photoanode surface. Via this strategy, efficient and robust CoO_x-modified TiO_2-TaON (CoO_x/TiO_2-TaON) photoanodes for water oxidation have been obtained.[17]

Among the state-of-the-art inorganic water oxidation catalysts, nickel oxide (NiO_x) being highly active and very robust appears to be an excellent choice as co-catalyst to be combined with *n*-type photoanodes. However, the use of nickel oxides for this purpose has been quite limited so far, notwithstanding some promising reports on improvement of the performance of Si,[22] TiO_2,[23] WO_3,[24] Ta_2O_5[25] and $BiVO_4$[26] photoanodes when modified with NiO_x. The aim of the present study is to apply electro- and photo-electrodeposition to fabricate NiO_x-modified TiO_2-TaON photocatalysts (NiO_x/TiO_2-TaON) and to probe the influence of the deposition conditions on the capacity of the resulting anodes to oxidize water. The catalytic activity has been examined using (photo)electrochemical methods and changes in microstructure during long-term testing probed using scanning electron microscopy (SEM). This is the first report on coupling a NiO_x electrocatalyst and TaON-based light harvesters.

Results and Discussion

Preparation, morphology and transient photocatalytic activity of the NiO_x/TiO_2-TaON anodes

Fabrication of the multi-component anodes was accomplished *via* consecutive functionalization of the TaON films screen-printed on a fluorine-doped tin oxide (FTO) support with titanium and nickel oxides. The importance of using TaON post-necked with TiO_2 (TiO_2-TaON) for stable and efficient operation of the photoanodes has been highlighted elsewhere.[15, 17] Post-necking was achieved *via* heat-decomposition of $TiCl_4$ drop-casted from an ethanol solution on a TaON film. Functionalization of TiO_2-TaON with the NiO_x water oxidation catalyst was carried out by using conventional and photo-assisted oxidative electrodeposition. In this process, oxidation of dissolved Ni^{2+} precursor in slightly alkaline solutions produces poorly soluble nickel oxide particles that are immobilized on the electrode surface.

Previous reports[17-18, 21a] have demonstrated the utility of the photo-assisted approach for the selective deposition of the CoO_x and MnO_x co-catalysts on *n*-type semiconductor surfaces. Surprisingly, examination of the SEM micrographs for the TiO_2-TaON photoanodes modified with NiO_x revealed that, for the (photo)electrolysis times used here (t_{dep} ≤ 60 s), deposition occurs on the TiO_2-TaON rather than the TaON-free FTO surface irrespective of the irradiation conditions (Fig. 1 and S1).

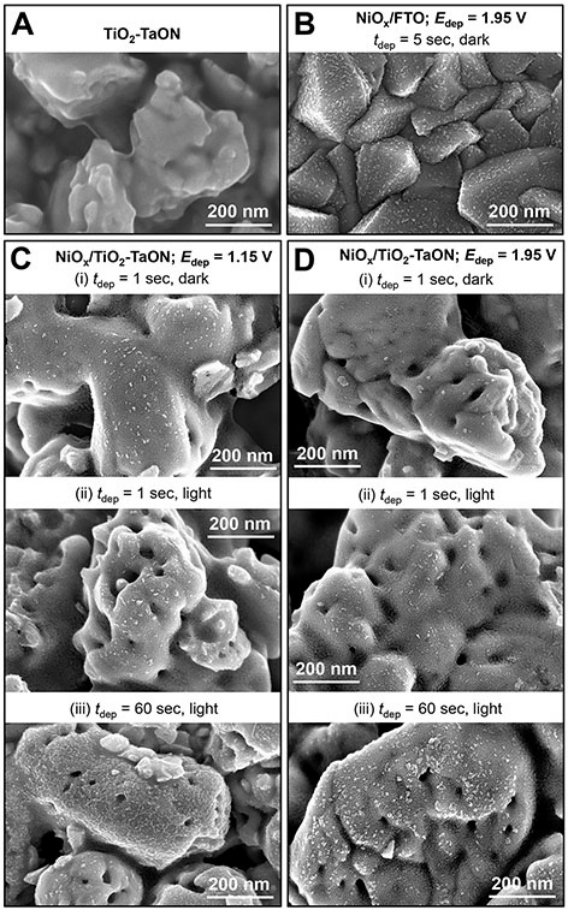

Figure 1. SEM micrographs for the (A) TiO_2-TaON, (B) NiO_x/FTO and (C, D) NiO_x/TiO_2-TaON films. NiO_x was electrodeposited in the dark or under illumination (1 sun, λ > 400 nm) from 0.5 mM $Ni(CH_3COO)_2$ in 0.1 M borate buffer (pH = 9.2) using the conditions defined in the figure panels.

SEM analysis of the electrode surfaces revealed that NiO_x particles could only be detected on areas covered with tantalum oxynitride even when a very positive deposition potential of 1.95 V was applied. Under these deposition conditions (t_{dep} = 1 s, E_{dep} = 1.95 V), irradiating the electrode surface with 100 mW cm^{-2} light with λ > 400 nm (hereinafter, visible irradiation) allowed the deposition of more electroactive NiO_x than in the dark, as deduced from comparisons of the corresponding cyclic voltammograms (Fig. 2A). In particular, the charge associated with the characteristic NiO_x voltammetric signals, which are manifested in the 1.2-1.6 V range (presumably, associated with the surface-confined $Ni^{II/III}$ redox process[23, 27]) and subsequent water electrooxidation catalytic current densities are higher for NiO_x/TiO_2-TaON produced under irradiation. With the same short deposition time of 1 s, but at much less positive E_{dep} of 1.15 V, the

influence of irradiation on the amount of electroactive NiO_x deposited was less pronounced (Fig. 2A), as also suggested by local energy dispersive X-ray (EDX) analysis undertaken under the SEM conditions (Fig. S1). Generally, using shorter t_{dep} and less positive E_{dep} produced lower NiO_x loadings on the TiO_2-TaON photoanode surface under both irradiated and dark conditions, as confirmed by SEM/EDX (Figs. 1 and S2), and voltammetric analyses (Fig. 2 and Table S1), as well as differences in charge passed during (photo)electrodeposition (Fig. S3).

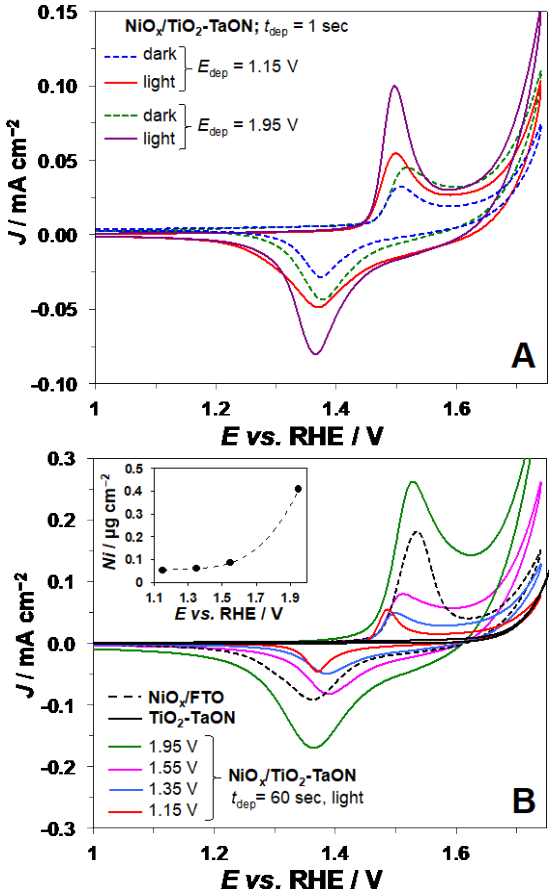

Figure 2. Dark cyclic voltammograms (scan rate, v = 0.025 V s^{-1}) for the NiO_x/TiO_2-TaON (*colored* curves), NiO_x/FTO (*black*, dashed curve) and TiO_2-TaON (*black*, solid curve) films immersed in 0.1 M borate buffer (pH 9.2). NiO_x was electrodeposited for t_{dep} = 1 (A) or 60 s (B) in the dark (dashed curves) or under 1 sun visible light illumination (solid curves) from 0.5 mM $Ni(CH_3COO)_2$ in 0.1 M borate buffer (pH = 9.2) under the conditions defined in the figure panels. Inset shows the surface concentration of Ni estimated using the average of the oxidation and reduction charges associated with the $Ni^{II/III}$ process and Faraday's law.

Quantification of the amount of electroactive NiO_x on the electrode surface is possible by applying the Faraday law to the charge associated with the $Ni^{II/III}$ process (Fig. 2), as described by Boettcher *et al.*[27c] By using this approach, the surface concentration of Ni was estimated to be quite low, varying within the 0.05-0.4 μg_{Ni} cm^{-2} range (hereinafter, surface concentrations and current densities are normalized to the geometric surface area of the electrode) depending on deposition conditions (see inset to Fig. 2B and Table S1). Quantitative analysis of the deposition transients to calculate the amount of NiO_x produced was not possible because of the contribution of water oxidation to the 'deposition' current/charge,[27a, 27b] especially, under irradiation (Fig. S3B).[17-18] More importantly, comparisons of the data presented in Fig. S3B provide initial evidence of significant photo-oxidative catalytic activity of the produced NiO_x/TiO_2-TaON anodes.

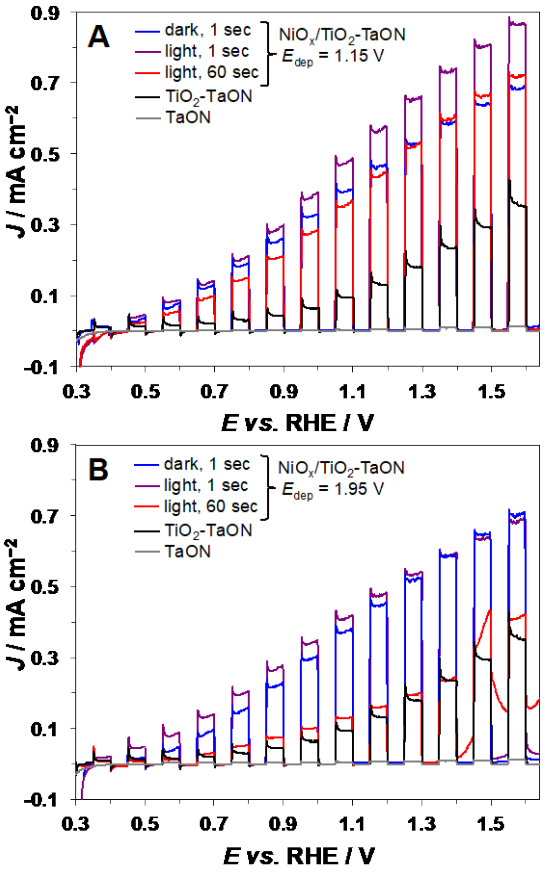

Figure 3. Voltammograms (v = 0.025 V s^{-1}) obtained under chopped visible light irradiation (1 sun, λ > 400 nm) for the NiO_x/TiO_2-TaON, TiO_2-TaON and TaON films in contact with 0.1 M borate buffer (pH 9.2). Electrodeposition of NiO_x was carried out using c_{Ni} = 0.5 mM at E_{dep} = 1.15 (A) or 1.95 V (*vs.* RHE) (B) in the dark or under illumination for the defined t_{dep}.

Figure 3 features voltammograms for water photo-electrooxidation measured under chopped visible light irradiation for a selection of NiO_x/TiO_2-TaON photoanodes prepared under different conditions. Consistent with the reports on IrO_2-,[12e, 28] CoO_x-,[13c, 17, 21a, 26a, 29] and MnO_x-modified[18] *n*-type semiconductors, a synergistic effect of coupling the NiO_x co-catalyst with the TaON photoanode enhances the water photo-oxidation performance. As noted previously,[15, 17-18] the preparation conditions determine the morphology and location of the co-catalyst (Fig. 3) and influence the performance.

To establish the electrodeposition parameters that produce the highest photo-oxidation current densities, extensive studies of the influence of E_{dep}, t_{dep} and concentration of the nickel acetate precursor (c_{Ni}) on the photocatalytic capacity of NiO_x/TiO_2-TaON were undertaken. The photocurrent densities derived from these voltammetric and chronoamperometric experiments are summarized in Figs. 4 and S4, respectively.

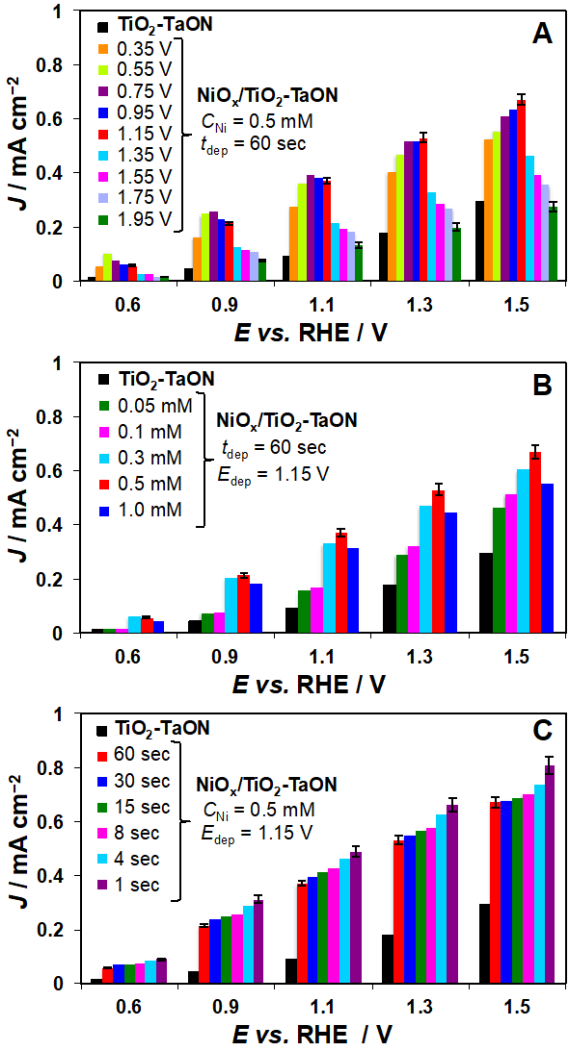

Figure 4. Water photo-electrooxidation current densities derived from voltammetric data obtained under chopped visible light irradiation (1 sun, λ > 400 nm) for the NiO_x/TiO_2-TaON and TiO_2-TaON films immersed in 0.1 M borate buffer (pH 9.2). The effect of the electrodeposition parameters, *viz.* E_{dep} (A), c_{Ni} (B) and t_{dep} (C) is shown. NiO_x was electrodeposited from $Ni(CH_3COO)_2$ solutions under illumination. Error bars show standard deviations calculated for at least 3 measurements.

The dependence of the photo-oxidative current densities on E_{dep} and c_{Ni} exhibit maxima at 1.15 V (Figs. 4A and S4A) and 0.5 mM (Figs. 4B and S4B), respectively. Applying these optimized conditions, the effect of t_{dep} on the activity was studied further. Interestingly, a gradual increase in the photocatalytic activity was observed with decreasing t_{dep} down to 1 sec (Figs. 4C and S3C). This observation suggests that comparatively low NiO_x loadings are sufficient to boost the water oxidation activity of TiO_2-TaON and that high amounts of the co-catalyst might block light absorption.[17-18] Agglomeration of NiO_x particles at higher loadings (*cf.* micrographs for t_{dep} = 1 and 60 s in Fig. 1) might also contribute to lower performance. Use of t_{dep} below 1 s resulted in poor reproducibility of the experiments, especially when undertaking depositions under illumination where concerted operation of potentiostat and solar simulator is needed. Thus, the optimized electrodeposition conditions were defined as E_{dep} = 1.15 V, c_{Ni} = 0.5 mM and t_{dep} = 1 sec; by using the voltammetric data, the corresponding loading of Ni was estimated as 0.01 wt.% with respect to TaON (see Table S1). The NiO_x/TiO_2-TaON films fabricated using this set of parameters outperformed the parent TiO_2-TaON photoanodes by a factor of *ca* 3-6 fold within the potential range relevant to Figs. 3-4. As for the MnO_x- and CoO_x-modified TiO_2-TaON,[17-18] the greatest enhancements in water photo-electrooxidation catalyzed by NiO_x/TiO_2-TaON were achieved at negative overpotentials, *i.e.* at potentials less positive than 1.23 V.

In accord with previous reports,[17-18] screening studies on NiO_x/TiO_2-TaON indicated that the loading of co-catalyst has a significant impact on the water oxidation activity. Photo-assisted electrodeposition under optimized conditions allowed appreciable enhancements in transient photocatalytic activity as against samples obtained in the dark (Fig. 3A). This may reflect a more favorable arrangement of the NiO_x particles with respect to the photoactive TaON sites in the former photoanode.

The charge transfer properties of the NiO_x/TiO_2-TaON photoanodes were probed with electrochemical impedance spectroscopy (EIS). There were only minor differences in the Nyquist plots for the bare and NiO_x-modified TiO_2-TaON catalyst films in the dark, as expected for such very low NiO_x loadings (Fig. S5). In contrast, a notable decrease in the impedance upon electrodepositing NiO_x on the photoanode surface was revealed when EIS analysis was undertaken under irradiation (Fig. S5). This behavior is consistent with that observed for the CoO_x/TiO_2-TaON photocatalysts[17] and is interpreted in terms of facilitated charge transfer at the semiconductor electrode|electrolyte interface where water oxidation occurs. On a semi-quantitative level, the EIS data for NiO_x/TiO_2-TaON under irradiation correlate well with the voltammetric and chronoamperometric measurements, *i.e.,* lower impedance is observed when higher photo-oxidation current densities are achieved.

In summary, the SEM/EDX analysis and (photo)-electrochemical studies confirm that functionalization of the TiO_2-TaON photoanodes with NiO_x enhances transient photo-oxidative capacity of the films, as proposed in Scheme 1. Selective formation of NiO_x on the TiO_2-TaON rather TaON-free FTO surface is possible *via* electrodeposition, both in the dark and under irradiation, which is unexpectedly dissimilar to our previous findings for the CoO_x and MnO_x deposition where illumination was always needed to achieve selective deposition on the TaON surface.[17-18] Nevertheless, the utility of using a photo-assisted deposition method for producing more active photoanodes was also revealed for the NiO_x/TiO_2-TaON system.

Long-term performance of NiO_x/TiO_2-TaON

As noted in the literature,[12e, 13c, 15, 17-18] photo-oxidative self-degradation of TaON is one major issue defining the less than satisfactory performance of the water-splitting photoanodes based on this semiconductor. Short diffusion lengths of the photo-generated holes have been suggested as a main cause for this,[3b, 12e, 13a] and addition of a water oxidation co-catalyst, NiO_x in this study, should lead to significant improvements. Indeed, a notable enhancement in the transient photo-oxidation activity was possible upon introduction of NiO_x onto the TiO_2-TaON surface (Figs. 3-4). However, the stability of the resulting photoanodes needed to be assessed, *e.g.*, by using a chronoamperometric technique.

Initially, in the course of the deposition optimization studies, the short-term stability of the NiO_x/TiO_2-TaON films was examined at the harsh potential of 1.5 V using chopped visible light

irradiation (Figs. S4 and S6). Although a substantial improvement in the robustness of TiO_2-TaON was possible upon functionalization with NiO_x, the modified electrodes still suffered from slow and continuous degradation under these strongly oxidizing conditions. Photoanodes containing higher loadings of NiO_x were more stable, but their activity was two or more times poorer than that of NiO_x/TiO_2-TaON obtained under optimized conditions (Figs. S4 and S6). No obvious influence of using the photo-assisted electrodeposition method as opposed to the conventional dark electrodeposition on the short-term stability of the photoanodes was found.

To examine the influence of electrodeposition conditions on the long-term performance of the NiO_x-modified TiO_2-TaON films, further chronoamperometric experiments were undertaken under continuous visible light irradiation and by applying a less positive potential of 1.15 V, which corresponds to *ca* −0.08 V overpotential for water oxidation (Fig. 5). Similar photocurrent densities for water oxidation were generated by the NiO_x/TiO_2-TaON films prepared in either the dark or under irradiation at E_{dep} = 1.15 V for t_{dep} = 1 s. Notably, they exceeded those produced by the samples prepared using E_{dep} = 1.95 V and/or t_{dep} = 60 s (Figs. 5A and S7), consistent with the outcomes of transient voltammetric measurements (Figs. 3-4). However, the slow and continuous degradation was again revealed for all NiO_x/TiO_2-TaON examined herein, as best exemplified by the 16 h measurements shown in Fig. 5B. During the first hour, the best performing samples (E_{dep} = 1.15 V, t_{dep} = 1 s, c_{Ni} = 0.5 mM, dark or irradiated deposition) suffered approximately 40% loss in performance, which extended to almost 75% degradation after 16 h. We note here that the photo-oxidative current measured during chronoamperometric experiments shown in Fig. 5 cannot be attributed to oxidation of Ni and is most probably solely due to water oxidation. Indeed, previous reports have convincingly demonstrated near 100% selectivity of the TaON-based photo- anodes for water oxidation.[12e, 13a, 13c, 17, 30] Moreover, the amount of Ni on the electrodes examined here is at least 3 orders of magnitude lower than that needed to sustain the charge passed during our photo-electrocatalytic experiments.

In attempt to establish the cause of the continuous degradation of NiO_x/TiO_2-TaON, SEM was used to examine the photoanodes after the long-term stability measurements (Fig. 6). Microscopic analysis revealed that the highly-dispersed NiO_x nanoparticles obtained using t_{dep} = 1 s (typical size below 10 nm) agglomerate into coarse flake-like structures (extending to several dozen nm in size) during water photo-electrooxidation. At higher co-catalyst loadings (obtained with t_{dep} = 60 s), the coarser flake morphology also becomes more dominant as compared to the freshly prepared catalysts (*cf.* Figs. 1 and 6). These unfavorable transformations probably occur *via* a dissolution/redeposition mechanism, which is commonly encountered with the non-noble transition metal oxide catalysts for water electrooxidation.[17-18, 30-31]

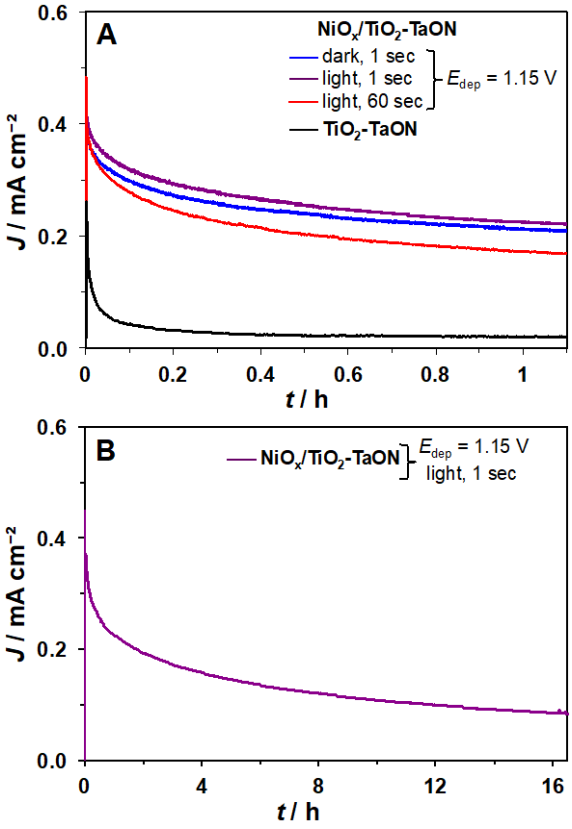

Figure 5. Water photo-electrooxidation at 1.15 V *vs.* RHE under continuous visible light irradiation (1 sun, λ > 400 nm) catalyzed by the NiO_x/TiO_2-TaON (*blue*, *purple*, *red*) and TiO_2-TaON (*black*) anodes immersed in 0.1 M borate buffer (pH 9.2) for (A) 1.1 and (B) 16.5 h. Electrodeposition of NiO_x was carried out using c_{Ni} = 0.5 mM, E_{dep} = 1.15 V and t_{dep} = 1 (*blue*) or 60 s (*red*) in the dark (*blue*) or under illumination (1 sun, λ > 400 nm) (*red, purple*).

A possible implication of the observed structural changes might be exposure of some of the photoactive tantalum oxynitride sites to the solution upon dissolution of the hole-scavenging co-catalyst and its subsequent redeposition on another NiO_x particle, rather than TaON. This would immediately reduce the stability (*cf.* data for unmodified TiO_2-TaON and NiO_x/TiO_2-TaON in Figs. 5, S4 and S6). One would have anticipated that increasing the NiO_x loading might remedy this problem, but surprisingly, degradation rates for NiO_x/TiO_2-TaON obtained using t_{dep} = 1 and 60 s were very similar (Fig. 5). Thus, additional factors seem to contribute to the instability of the TiO_2-TaON photoanodes functionalized with NiO_x. One plausible explanation is provided below.

The type of conductivity of nickel oxides undergoes change from *p*-type for NiO ($Ni(OH)_2$) to *n*-type for NiOOH and higher oxidation states NiO_x, the latter being relevant to the water oxidation catalysis.[32] Therefore, there is no efficient mechanism for transfer of the holes photo-generated at the *n*-type TaON surface through the *n*-type NiO_x co-catalyst. Most probably, NiO_x is oxidized at the *n*|*n* interface and most efficient water photo-electrooxidation should be at this interface rather than on the surface of NiO_x. This also explains the virtue of having exceptionally low loadings of highly-dispersed separated NiO_x particles for the best performing NiO_x/TiO_2-TaON photoanodes. However, this process is too slow (most probably due to sluggish kinetics of the OER) to scavenge photo-generated holes from TaON at a rate needed to prevent self-degradation of the

photoactive material, as confirmed by our data summarized above. This might be one of the main reasons for unsatisfactory stability of NiO_x/TiO_2-TaON (Fig. 5). Coupled to a continuous dissolution/redeposition of NiO_x, this may lead to significant number of the photoactive TaON surface sites being unprotected during water photo-electrooxidation. All NiO_x/TiO_2-TaON materials persistently degrade at potentials above 1.0 V and stabilization in performance has not been achieved even after 16 h (Fig. 5B). Notably, (photo)electrodeposited MnO_x, which is also an *n*-type semiconductor,[33] is not capable of maintaining a satisfactory long-term stability of the TiO_2-TaON photoanodes at positive potentials.[18]

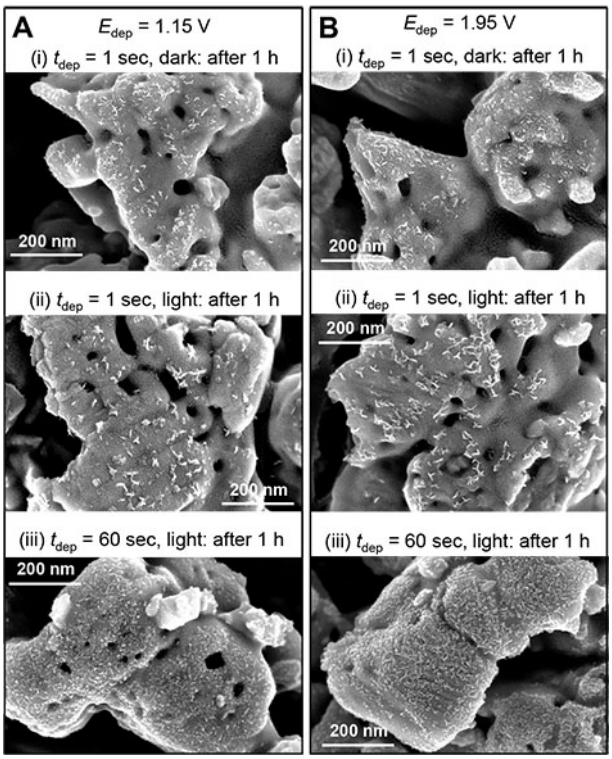

Figure 6. SEM micrographs obtained for the NiO_x/TiO_2-TaON films after chronoamperometric measurements at 1.15 V *vs.* RHE under continuous visible light irradiation (other conditions were as defined in Figs. 5 and S6). Electrodeposition conditions for NiO_x over the TiO_2-TaON films were as defined in the figure and caption to Fig. 2.

In contrast, Kisch and co-authors[34] were one of the first to emphasize the advantages of a *p*|*n* junction at the interface between the photoactive semiconductor (*n*-type $BiVO_4$) and a co-catalyst (*p*-type Co_3O_4) for water splitting applications. This approach was recently extended by Domen and co-workers[26a], who were able to enhance the water photo-electrooxidation performance by introducing a thin *p*-type NiO layer on $BiVO_4$ or CoO_x-modified $BiVO_4$. These findings suggest that a *p*|*n* junction facilitates the extraction of the photo-generated holes from the *n*-type light-harvesting semiconductor. This should be especially important for the (oxy)nitride-based photoanodes like TaON and Ta_3N_5, which are very prone to photo-oxidative degradation.[13c, 17, 26a] A comprehensive scrutiny of the Ta_3N_5 photoanodes modified with hole-scavenging and storing ferrihydrite layers by Li and co-workers[35] confirms this supposition.

Photocatalytic efficiency of the functionalized TiO_2-TaON anodes

Incident photon-to-current conversion efficiency (IPCE) measurements were undertaken to quantify the capacity of the photoanodes under study to transform visible irradiation of different wavelengths into water photo-oxidation current. The efficiency was calculated as[4]

$$\mathrm{IPCE}(\lambda) = 1240\,\frac{J}{\lambda P_{\mathrm{mono}}},$$

where 1240 / J C^{-1} nm is the product of the Planck's constant and the speed of light divided by electron charge, J / A cm^{-2} is the photocurrent density derived from voltammograms (scan rate 0.005 V s^{-1}) measured under chopped irradiation, λ / nm and P_{mono} / W cm^{-2} are wavelength and intensity of the monochromatic light, respectively.

Representative IPCE plots constructed for the best-performing NiO_x/TiO_2-TaON films are compared to those for the parent TiO_2-TaON films in Fig. 7. The sum of the photocurrent densities obtained under monochromatic light irradiation (λ from 410 to 530 nm) is consistent with that measured under non-filtered visible light irradiation (1 sun, λ > 400 nm). As expected, and found previously for the CoO_x- and MnO_x-modified TiO_2-TaON photoanodes, introduction of the NiO_x co-catalyst does not qualitatively change the IPCE profile of TaON. The IPCE values are higher at more positive potentials, but it is more informative to compare efficiencies of the photoanodes at negative OER overpotentials (*i.e.* potentials < 1.23 V *vs.* RHE). For example, the IPCE is 7.5 % at 0.9 V and λ = 410 nm for NiO_x/TiO_2-TaON, which reflects significant enhancement in efficiency, *cf.* <0.4 % provided by TiO_2-TaON.

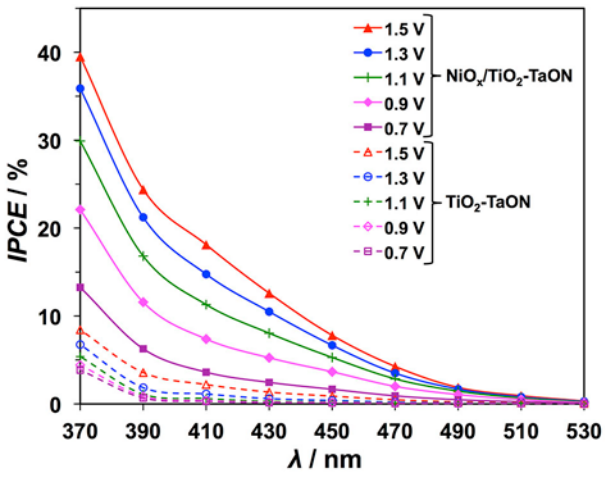

Figure 7. IPCE spectra at defined potentials (*vs.* RHE) for the NiO_x/TiO_2-TaON (solid curves) and TiO_2-TaON (dashed curves) films immersed in 0.1 M borate buffer (pH 9.2). Photo-electrodeposition (1 sun, λ > 400 nm) of NiO_x was undertaken using c_{Ni} = 0.5 mM, E_{dep} = 1.15 V and t_{dep} = 1 s.

To account for the fact that the NiO_x/TiO_2-TaON catalysts need additional driving force, *viz.* applied potential, to generate appreciable water photo-oxidation current, the efficiencies were also calculated as

$$\text{AB-PCE} = \frac{J(1.23-E)}{P},$$

where AB-PCE is applied bias-corrected photon-to-current conversion efficiency[2d], J / A cm^{-2} is the photocurrent density derived from the voltammetric data shown in Fig. 3, 1.23 V vs. RHE is the theoretical potential for water splitting, E / V is the applied potential vs. RHE, P / W cm^{-2} is the light intensity.

The AB-PCE *vs.* E plots for the selected NiO_x/TiO_2-TaON photoanodes and the co-catalyst-free TiO_2-TaON film are compared in Fig. S8. All NiO_x/TiO_2-TaON examined show the best AB-PCEs at 0.9 V irrespective of the NiO_x deposition conditions. The electrodes produced under optimized conditions (c_{Ni} = 0.5 mM, E_{dep} = 1.15 V, t_{dep} = 1 s) exhibit the efficiency of 0.1% at 0.9 V, which is at least an order of magnitude higher than for TiO_2-TaON.

Comparisons of the data above with the outcomes of our previous studies lead to the conclusion that use of the NiO_x co-catalyst to functionalize the TiO_2-TaON photoanodes is more advantageous than MnO_x ($IPCE_{410\ nm}$ = 5.9% and AB-PCE = 0.085% at 0.9 V).[18] At the same time, the NiO_x-functionalized photo-electrocatalysts exhibit notably lower efficiencies than the CoO_x/TiO_2-TaON films fabricated under optimized conditions ($IPCE_{410\ nm}$ = 16% and AB-PCE = 0.25% at 0.9 V).[17] The transient nature of the IPCE and AB-PCE values reported here should be also considered when comparing to the efficiencies of other photoanodes.

Conclusions

The present work further extends our studies[12e, 13c, 14-15, 17-18, 30] on the effect of coupling the TaON photocatalyst to the best water oxidation electrocatalysts based on the abundant elements discovered to date. Extensive optimization experiments for (photo)electrodeposition of the NiO_x co-catalyst onto the TiO_2-postnecked TaON films reported herein further highlight intricate interrelations between the charge-transfer properties, catalytic performance and microstructure for this class of multicomponent photoanodes. The fast (photo)electrodeposition method employed to immobilize NiO_x over the TiO_2-TaON surface allows a 6-fold enhancement in photocurrent densities for NiO_x/TiO_2-TaON films when compared to TiO_2-TaON. However, the NiO_x-functionalized TiO_2-TaON photoanodes suffer continuous degradation, most probably due to insufficient capacity of the *n*-type co-catalyst to withdraw photo-generated holes from TaON. We suggest that most significant improvements in the water photo-oxidation activity of the TaON-based anodes require a properly engineered *p*|*n* interface between the photoactive semiconductor and an electrooxidation co-catalyst. This is possible when a *p*-type CoO_x electrocatalyst is deposited on TiO_2-TaON,[17] but is most probably unachievable with *n*-type manganese oxides and nickel oxides.

Experimental Section

Materials

All chemicals were purchased from either Sigma Aldrich or Merck and used as received. Water used in all experiments was pre-purified by reverse osmosis.

Thin (*ca* 1.5 μm) mesoporous TaON films (0.2 cm^2 geometric surface area; 1 mg_{TaON} cm^{-2} loading) were immobilized on glass coated with fluorine-doped tin oxide (FTO; sheet resistance 10 Ω cm^{-2}; Dyesol, Australia) using a screen-printing method following the procedures reported elsewhere.[13b, 15] Post-necking of the screen-printed TaON with *ca* 15 wt.% TiO_2 to produce TiO_2-TaON electrodes was achieved by applying 20 μL of 20 mM $TiCl_4$ solution in ethanol and subsequent heating in an air flow at 450°C.[15]

Photo-electrochemical methods

A Zahner-Elektrik PECC-1 photo-electrochemical cell connected to a Bio-Logic VSP modular potentiostat was used to carry out all experiments at ambient temperature (25 ± 1°C). A 150 W Xe-arc lamp (with a horizontal light beam) fitted to a Newport-Oriel solar simulator was used as a light source. An AM 1.5G filter and a long pass filter (λ > 400 nm) were used to simulate the solar spectrum and to provide visible light irradiation, respectively. A light intensity of 1 sun, which corresponds to 100 mW cm^{-2}, was achieved using neutral density filters and measured by a calibrated Hamamatsu S1133 photoactive diode connected to a multimeter. To measure the incident photon-to-current conversion efficiency (IPCE), a series of band pass filter (average band-width 10 nm) was used instead of the long pass filter and neutral density filters. The corresponding light intensities were also measured using the photoactive diode.

Freshly prepared FTO/glass substrate, bare or modified with a (photo)catalyst layer, and a high surface area Pt wire were used as working and auxiliary electrodes, respectively. The reference electrode was Ag|AgCl|KCl(sat.) (BAS) with $E^0_{Ag|AgCl}$ = 0.197 V *vs.* normal hydrogen electrode (NHE). However, all potentials are reported *versus* reversible hydrogen electrode (RHE), which potential was calculated as E_{RHE} = -0.059pH V *vs.* NHE = -0.059pH - 0.197 V *vs.* Ag|AgCl. All currents are reported normalized to the geometric surface area of the electrochemically active films. An aqueous sodium borate buffer (0.10 M, pH = 9.2) was employed as supporting electrolyte in all photo-electrochemical measurements.

$Ni(CH_3COO)_2$ dissolved in the supporting electrolyte solution was used for the (photo)electrodeposition of NiO_x on the TiO_2-TaON or bare FTO substrates under either visible light irradiation or in the dark. Electrodeposition was carried out in a constant potential mode. The electrode area around the TiO_2-TaON film was masked with a polyimide tape (Kapton) to avoid electrodeposition on the TaON-free surface. The same mask was used for the deposition of 0.2 cm^2 NiO_x films on the bare FTO substrate. The precursor concentration (c_{Ni}), deposition potential (E_{dep}), and duration (t_{dep}) were varied in the ranges 0.05-1.0 mM, 0.35-1.95 V *vs.* RHE and 1-60 s, respectively.

Microscopic analysis

The morphology of the catalyst layers was examined before and after photo-electrochemical testing using a field-emission scanning electron microscope FEI Magellan 400 FEG. EDX was used for local elemental analysis. Samples for the SEM/EDX analysis were prepared by mounting the electrodes over the SEM specimen stubs using a carbon tape and were coated with iridium (*ca* 2-3 nm thick).

Acknowledgements

The authors acknowledge the Australian Research Council for providing funds to support this work through ARC Centre of Excellence for Electromaterials Science (Grant No. CE140100012). We also thanks to the School of Chemistry (Monash University) for providing research facilities and scholarships and the Monash Centre for Electron Microscopy (Monash University) for providing microscopy facilities.

Keywords: tantalum oxynitride • nickel oxide • cobalt oxide • water photo-oxidation • electrodeposition

[1] a) T. Pregger, D. Graf, W. Krewitt, C. Sattler, M. Roeb, S. Möller, *Int. J. Hydrogen Energy* **2009**, *34*, 4256-4267; b) Y. Yamada, *Int. J. Hydrogen Energy* **2003**, *28*, 1167-1169; c) A. S. Joshi, I. Dincer, B. V. Reddy, *Int. J. Hydrogen Energy* **2011**, *36*, 11246-11257; d) A. Kudo, *Pure Appl. Chem.* **2007**, *79*, 1917-1927; e) K. J. Young, L. A. Martini, R. L. Milot, R. C. Snoeberger, V. S. Batista, C. A. Schmuttenmaer, R. H. Crabtree, G. W. Brudvig, *Coord. Chem. Rev.* **2012**; f) S. Licht, B. Wang, S. Mukerji, T. Soga, M. Umeno, H. Tributsch, *Int. J. Hydrogen Energy* **2001**, *26*, 653-659; g) G. Peharz, F. Dimroth, U. Wittstadt, *Int. J. Hydrogen Energy* **2007**, *32*, 3248-3252; h) S. A. Bonke, M. Wiechen, D. R. MacFarlane, L. Spiccia, *Energy Environ. Sci.* **2015**, *8*, 2791-2796.

[2] a) A. Fujishima, K. Honda, *Nature* **1972**, *238*, 37-38; b) J. Sun, D. K. Zhong, D. R. Gamelin, *Energy Environ. Sci.* **2010**, *3*, 1252-1261; c) L. Li, L. Duan, Y. Xu, M. Gorlov, A. Hagfeldt, L. Sun, *Chem. Commun.* **2010**, *46*, 7307-7309; d) T. Hisatomi, J. Kubota, K. Domen, *Chem. Soc. Rev.* **2014**, *43*, 7520-7535; e) X. Chen, S. Shen, L. Guo, S. S. Mao, *Chem. Rev.* **2010**, *110*, 6503-6570.

[3] a) M. G. Walter, E. L. Warren, J. R. McKone, S. W. Boettcher, Q. Mi, E. A. Santori, N. S. Lewis, *Chem. Rev.* **2010**, *110*, 6446-6473; b) R. Abe, *J. Photochem. Photobiol., C* **2010**, *11*, 179-209; c) H. Kisch, *Angew. Chem. Int. Ed.* **2013**, *52*, 812-847.

[4] O. K. Varghese, C. A. Grimes, *Sol. Energy Mater. Sol. Cells* **2008**, *92*, 374-384.

[5] a) J. A. Turner, *Science* **1999**, *285*, 687-689; b) K. Rajeshwar, *J. Appl. Electrochem.* **2007**, *37*, 765-787; c) K. Rajeshwar, R. McConnell, S. Licht, *Solar hydrogen generation-toward a renewable energy future*, Springer Science and Business Media, New York, **2008**; d) J. R. Bolton, S. J. Strickler, J. S. Connolly, *Nature* **1985**, *316*, 495-500.

[6] a) Z. Yu, F. Li, L. Sun, *Energy Environ. Sci.* **2015**, *8*, 760-775; b) X. Li, J. Yu, J. Low, Y. Fang, J. Xiao, X. Chen, *J. Mater. Chem. A* **2015**, *3*, 2485-2534.

[7] M. A. Rahman, S. Bazargan, S. Srivastava, X. Wang, M. Abd-Ellah, J. P. Thomas, N. F. Heinig, D. Pradhan, K. T. Leung, *Energy Environ. Sci.* **2015**.

[8] a) Y. Xu, M. A. A. Schoonen, *Am. Mineral.* **2000**, *85*, 543-556; b) X. Lu, S. Xie, H. Yang, Y. Tong, H. Ji, *Chem. Soc. Rev.* **2014**, *43*, 7581-7593; c) M. Long, W. Cai, J. Cai, B. Zhou, X. Chai, Y. Wu, *J. Phys. Chem. B* **2006**, *110*, 20211-20216; d) W. J. Chun, A. Ishikawa, H. Fujisawa, T. Takata, J. N. Kondo, M. Hara, M. Kawai, Y. Matsumoto, K. Domen, *J. Phys. Chem. B* **2003**, *107*, 1798-1803.

[9] F. Q. Xiong, J. Shi, D. Wang, J. Zhu, W. H. Zhang, C. Li, *Catal. Sci. Technol.* **2013**, *3*, 1699-1702.

[10] D. K. Zhong, J. Sun, H. Inumaru, D. R. Gamelin, *J. Am. Chem. Soc.* **2009**, *131*, 6086-6087.

[11] S. Tokunaga, H. Kato, A. Kudo, *Chem. Mater.* **2001**, *13*, 4624-4628.

[12] a) M. Higashi, R. Abe, K. Teramura, T. Takata, B. Ohtani, K. Domen, *Chem. Phys. Lett.* **2008**, *452*, 120-123; b) M. Higashi, R. Abe, T. Takata, K. Domen, *Chem. Mater.* **2009**, *21*, 1543-1549; c) R. Abe, T. Takata, H. Sugihara, K. Domen, *Chem. Commun.* **2005**, 3829-3831; d) Y. Wu, P. Lazic, G. Hautier, K. Persson, G. Ceder, *Energy Environ. Sci.* **2013**, *6*, 157; e) R. Abe, M. Higashi, K. Domen, *J. Am. Chem. Soc.* **2010**, *132*, 11828-11829; f) M. Higashi, K. Domen, R. Abe, *J. Am. Chem. Soc.* **2013**, *135*, 10238-10241; g) A. Kasahara, K. Nukumizu, T. Takata, J. N. Kondo, M. Hara, H. Kobayashi, K. Domen, *J. Phys. Chem. B* **2003**, *107*, 791-797.

[13] a) M. Higashi, K. Domen, R. Abe, *Energy Environ. Sci.* **2011**, *4*, 4138-4147; b) G. Hitoki, T. Takata, J. N. Kondo, M. Hara, H. Kobayashi, K. Domen, *Chem. Commun.* **2002**, 1698-1699; c) M. Higashi, K. Domen, R. Abe, *J. Am. Chem. Soc.* **2012**, *134*, 6968-6971; d) S. S. K. Ma, K. Maeda, K. Domen, *Catal. Sci. Technol.* **2012**, *2*, 818-823.

[14] R. Abe, T. Takata, H. Sugihara, K. Domen, *Chem. Lett.* **2005**, *34*, 1162-1163.

[15] S. S. Gujral, A. N. Simonov, M. Higashi, R. Abe, L. Spiccia, *ChemElectroChem* **2015**, *2*, 1270-1278.

[16] a) S. Ito, T. N. Murakami, P. Comte, P. Liska, C. Grätzel, M. K. Nazeeruddin, M. Grätzel, *Thin Solid Films* **2008**, *516*, 4613-4619; b) P. M. Sommeling, B. C. O'Regan, R. R. Haswell, H. J. P. Smit, N. J. Bakker, J. J. T. Smits, J. M. Kroon, J. A. M. van Roosmalen, *J. Phys. Chem. B* **2006**, *110*, 19191-19197; c) C. B. Lee, *J. of Future Fusion Technology* **2009**, *1*, 43-46; d) A. Sedghi, H. N. Miankushki, *Int. J. Electrochem. Sci.* **2012**, *7*, 12078-12089.

[17] S. S. Gujral, A. N. Simonov, M. Higashi, X.-Y. Fang, R. Abe, L. Spiccia, *ACS Catal.* **2016**, DOI: 10.1021/acscatal.6b00629.

[18] S. S. Gujral, A. N. Simonov, X.-Y. Fang, M. Higashi, T. Gengenbach, R. Abe, L. Spiccia, *Catal. Sci. Technol.* **2016**, DOI: 10.1039/C5CY01432H

[19] E. S. Kim, N. Nishimura, G. Magesh, J. Y. Kim, J. W. Jang, H. Jun, J. Kubota, K. Domen, J. S. Lee, *J. Am. Chem. Soc.* **2013**, *135*, 5375-5383.

[20] K. Maeda, D. Lu, K. Domen, *Chem. Eur. J.* **2013**, *19*, 4986-4991.

[21] a) E. M. P. Steinmiller, K.-S. Choi, *Proc. Natl. Acad. Sci. U. S. A.* **2009**, *106*, 20633-20636; b) K. Maeda, *Phys. Chem. Chem. Phys.* **2013**, *15*, 10537-10548.

[22] a) K. Sun, S. Shen, J. S. Cheung, X. Pang, N. Park, J. Zhou, Y. Hu, Z. Sun, S. Y. Noh, C. T. Riley, P. K. L. Yu, S. Jin, D. Wang, *Phys. Chem. Chem. Phys.* **2014**, *16*, 4612-4625; b) K. Sun, N. Park, Z. Sun, J. Zhou, J. Wang, X. Pang, S. Shen, S. Y. Noh, Y. Jing, S. Jin, P. K. L. Yu, D. Wang, *Energy Environ. Sci.* **2012**, *5*, 7872-7877.

[23] F. Lin, S. W. Boettcher, *Nat. Mater.* **2014**, *13*, 81-86.

[24] a) T. Jin, P. Diao, D. Xu, Q. Wu, *Electrochim. Acta* **2013**, *114*, 271-277; b) Y.-H. Lai, T. C. King, D. S. Wright, E. Reisner, *Chem. Eur. J.* **2013**, *19*, 12943-12947.

[25] Y. Noda, B. Lee, K. Domen, J. N. Kondo, *Chem. Mater.* **2008**, *20*, 5361-5367.

[26] a) M. Zhong, T. Hisatomi, Y. Kuang, J. Zhao, M. Liu, A. Iwase, Q. Jia, H. Nishiyama, T. Minegishi, M. Nakabayashi, N. Shibata, R. Niishiro, C. Katayama, H. Shibano, M. Katayama, A. Kudo, T. Yamada, K. Domen, *J. Am. Chem. Soc.* **2015**, *137*, 5053-5060; b) T. W. Kim, K.-S. Choi, *Science* **2014**, *343*, 990-994.

[27] a) A. Singh, S. L. Y. Chang, R. K. Hocking, U. Bach, L. Spiccia, *Energy Environ Sci.* **2013**, *6*, 579-586; b) A. Singh, M. Fekete, T. Gengenbach, A. N. Simonov, R. K. Hocking, S. L. Y. Chang, M. Rothmann, S. Powar, D. Fu, Z. Hu, Q. Wu, Y.-B. Cheng, U. Bach, L. Spiccia, *ChemSusChem* **2015**, *8*, 4266-4274; c) L. Trotochaud, J. K. Ranney, K. N. Williams, S. W. Boettcher, *J. Am. Chem. Soc.* **2012**, *134*, 17253-17261.

[28] S. D. Tilley, M. Cornuz, K. Sivula, M. Gratzel, *Angew. Chem. Int. Ed. Engl.* **2010**, *49*, 6405-6408.

[29] F. F. Abdi, L. Han, A. H. Smets, M. Zeman, B. Dam, R. van de Krol, *Nat. Commun.* **2013**, *4*, 2195.

[30] M. Higashi, O. Tomita, R. Abe, *Top. Catal.* **2016**, DOI 10.1007/s11244-016-0548-4

[31] a) J. B. Gerken, J. G. McAlpin, J. Y. C. Chen, M. L. Rigsby, W. H. Casey, R. D. Britt, S. S. Stahl, *J. Am. Chem. Soc.* **2011**, *133*, 14431-14442; b) D. A. Lutterman, Y. Surendranath, D. G. Nocera, *J. Am. Chem. Soc.* **2009**, *131*, 3838-3839.

[32] a) M. K. Carpenter, D. A. Corrigan, *J. Electrochem. Soc.* **1989**, *136*, 1022-1026; b) G. Barral, F. Njanjo-Eyoke, S. Maximovitch, *Electrochim. Acta* **1995**, *40*, 2815-2828.

[33] B. A. Pinaud, Z. Chen, D. N. Abram, T. F. Jaramillo, *J. Phys. Chem. C* **2011**, *115*, 11830-11838.

[34] Long, Cai, H. Kisch, *J. Phys. Chem. C* **2008**, *112*, 548-554.

[35] G. Liu, J. Shi, F. Zhang, Z. Chen, J. Han, C. Ding, S. Chen, Z. Wang, H. Han, C. Li, *Angew. Chem. Int. Ed.* **2014**, *53*, 7295-7299.

Entry for the Table of Contents

FULL PAPER

The effect of functionalization of the TaON films with electrodeposited nickel oxides, NiO_x, on the photo-catalytic water oxidation by multi-component photoanodes is examined. Limitations of NiO_x as a co-catalyst are revealed, and strategies to create better TaON-based photoanodes are discussed.

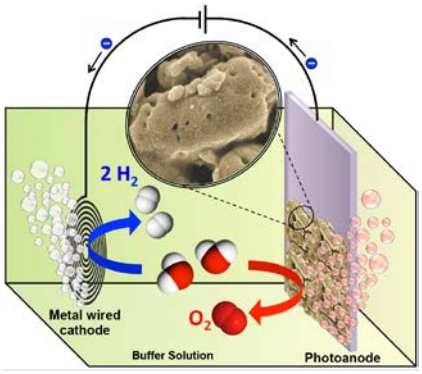

Satnam Singh Gujral, Alexandr N. Simonov, Xi-Ya Fang, Masanobu Higashi, Ryu Abe and Leone Spiccia**

Page No. – Page No.

Solar water oxidation by multi-component TaON photoanodes functionalized with nickel oxide